

Nonparametric Smoothing of Directional and Axial Data

Lutz Dümbgen¹ and Caroline Haslebacher^{1,2}

¹*University of Bern*

²*Southwest Research Institute, Boulder, Colorado, USA*

January 30, 2025

Abstract. We discuss generalized linear models for directional data where the conditional distribution of the response is a von Mises–Fisher distribution in arbitrary dimension or a Bingham distribution on the unit circle. To do this properly, we parametrize von Mises–Fisher distributions by Euclidean parameters and investigate computational aspects of this parametrization. Then we modify this approach for local polynomial regression as a means of nonparametric smoothing of distributional data. The methods are illustrated with simulated data and a data set from planetary sciences involving covariate vectors on a sphere with axial response.

AMS subject classification: 62J12, 62H11, 62G05

Key words: Bingham distributions, exponential family, Galileo mission, generalized linear model, local polynomial modelling, stereographic projection, von Mises–Fisher distributions.

1 Introduction

The starting point for the present paper are data sets from Planetary Sciences. The Galileo Mission yielded raw imaging data from the jovian¹ moons Ganymede and Europa. Both moons have a global subsurface ocean with an ice shell on top. From pictures of linear surface features on the icy surface, the physicists extracted observation pairs $(\mathbf{X}_i, \mathbf{V}_i)$, $1 \leq i \leq n$, consisting of a center position \mathbf{X}_i on the surface at which a feature, presumably a crack in the ice layer, could be identified, and the direction \mathbf{V}_i of that crack. Identifying the surface of the moon with the unit sphere \mathbb{S}^2 of \mathbb{R}^3 , we are talking about points $\mathbf{X}_i \in \mathbb{S}^2$ and $\mathbf{V}_i \in \mathbb{S}^2 \cap \mathbf{X}_i^\perp$, where \mathbf{V}_i represents the axis $\mathbb{R}\mathbf{V}_i$. Figures 1 and 2 illustrate this process for the moon Europa. Figure 1 shows a superposition of a basemap with a particular region highlighted. In addition one sees some fine structures on the icy surface which become visible when zooming in. By means of tailored classic and deep learning algorithms (Haslebacher et al., 2024, 2025) one can extract data pairs $(\mathbf{X}_i, \mathbf{V}_i)$ as described before, see Figure 2. The whole data set contains 5623 observation pairs in 19 different regions, but we only show 2184 of these pairs. The region in the foreground (black dots, green

¹of the planet Jupiter

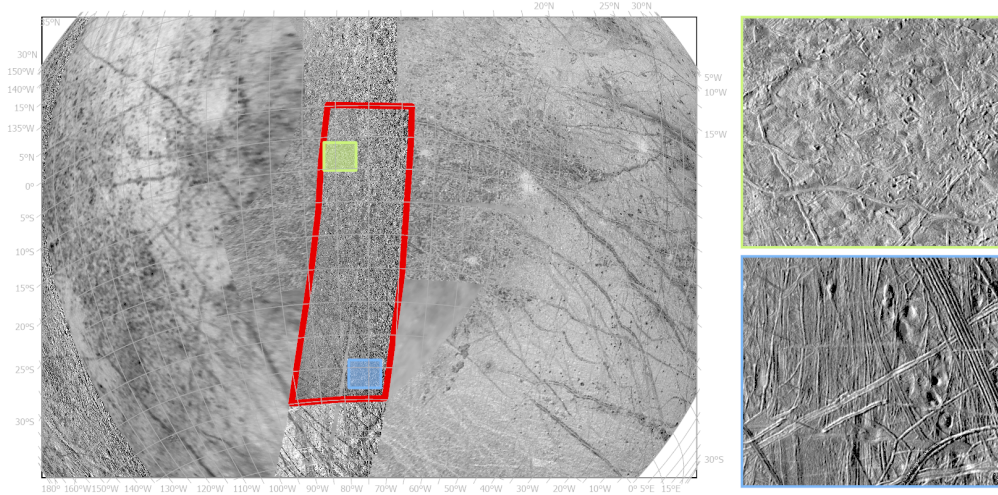


Figure 1: An image of Europa’s surface (left panel) and some fine structures.

lines) corresponds to the region with red boundary in Figure 1. It contains 2656 observations $(\mathbf{X}_i, \mathbf{V}_i)$, and we show a subset of 200 pairs.

The task was to smooth these noisy data and to determine for various points $\mathbf{x}_o \in \mathbb{S}^2$ whether there was a preferred axis direction of ice cracks close to \mathbf{x}_o . The existence and strength of preferred directions allows conclusions about physical properties of the moon, e.g. the link of tidal forces to ice cracks (Rhoden and Hurford, 2013). Translated into a mathematical task, we wanted to determine for such a point \mathbf{x}_o a Bingham distribution (Bingham, 1974) on the unit circle $\mathbb{S}^2 \cap \mathbf{x}_o^\perp$ of the tangent space \mathbf{x}_o^\perp of the unit sphere at \mathbf{x}_o .

When thinking about smaller subregions of the unit sphere \mathbb{S}^2 , one could approximate this by a subset of \mathbb{R}^2 , and the task looks *similar* to the task of smoothing directional data, given by pairs $(\mathbf{X}_i, \mathbf{Y}_i) \in \mathbb{R}^2 \times \mathbb{S}^1$, $1 \leq i \leq n$, where the conditional distribution of \mathbf{Y}_i , given \mathbf{X}_i , is a von Mises–Fisher distribution with parameters depending smoothly on \mathbf{X}_i . More generally, one could think about observations $(\mathbf{X}_i, \mathbf{Y}_i)$ with covariates \mathbf{X}_i in an arbitrary covariate space \mathcal{X} and directional responses $\mathbf{Y}_i \in \mathbb{S}^{d-1}$ for some $d \geq 2$.

Two general references about directional data, including regression methods, are the monograph of Mardia and Jupp (2000) and the review paper of Pewsey and García-Portugués (2021). These references describe and cite numerous approaches to regression with directional response. Some of these approaches involve transformations of the directional response into points in some Euclidean space, but the choice of this transformation is somewhat ad hoc. Let us restrict our attention to models in which $\mathbf{Y}_i \in \mathbb{S}^{d-1}$ has a von Mises–Fisher distribution conditional on \mathbf{X}_i . Many authors characterize a von Mises–Fisher distribution via a direction parameter $\boldsymbol{\beta} \in \mathbb{S}^{d-1}$ and a concentration parameter $\kappa \geq 0$ which is often viewed as a nuisance parameter, whereas $\boldsymbol{\beta}$ is the parameter of interest. We propose to replace such a parameter pair $(\boldsymbol{\beta}, \kappa)$ with the vector $\mathbf{z} = \kappa\boldsymbol{\beta} \in \mathbb{R}^d$. Since $\kappa = \|\mathbf{z}\|$ and $\boldsymbol{\beta} = \kappa^{-1}\mathbf{z}$, this description is equivalent, and dealing with parameters in a Euclidean space is more convenient, particularly in generalized linear models.

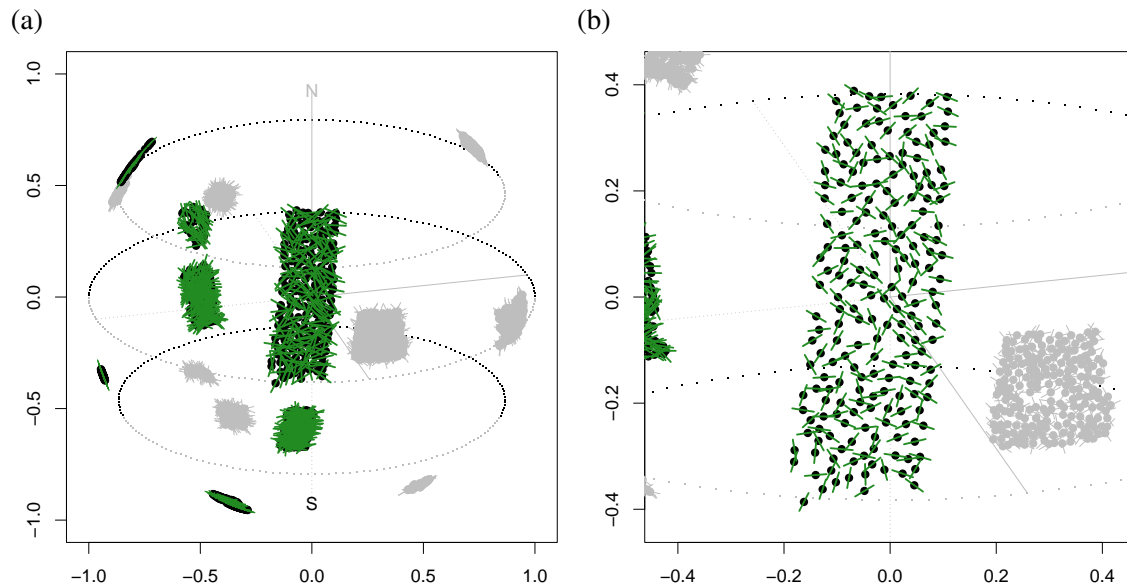


Figure 2: (a) Processed image data $(\mathbf{X}_i, \mathbf{V}_i)$ for Europa's surface. The points \mathbf{X}_i are shown as black dots, the axes \mathbf{V}_i are indicated by green line segments connecting $\mathbf{X}_i \pm 0.05 \cdot \mathbf{V}_i$. Observations on the backside are shown in gray. (b) The main cluster corresponds to the region highlighted in red in Figure 1.

The remainder of this paper is structured as follows. Section 2 starts with a short recap of von Mises–Fisher (vMF) distributions and Bingham (Bh) distributions on the unit sphere \mathbb{S}^{d-1} of \mathbb{R}^d . Then we describe a very useful connection between these two families for dimension $d = 2$. Finally, in view of the regression methods derived later, we provide some details about the numerical computation of the mean vector and covariance matrix of a von Mises–Fisher distribution. This involves exact formulae as well as approximations for parameter vectors with large norm and is potentially of independent interest.

Section 3 describes regression methods for data with directional response vectors. As a parametric approach, we propose generalized linear models (GLMs). For a thorough introduction and overview of this topic we refer to McCullagh and Nelder (1989). Thereafter we describe a modification of this parametric approach to local parametric modelling in the spirit of Fan et al. (1998). The latter method is illustrated with simulated data.

In Section 4 we explain how to apply the nonparametric methods of Section 3 to the specific data mentioned in the beginning, a key tool being stereographic projections of the covariate vectors $\mathbf{X}_i \in \mathbb{S}^2$ onto \mathbb{R}^2 and suitable transformations of the accompanying axes $\mathbf{V}_i \in \mathbb{S}^2 \cap \mathbf{X}_i^\perp$ into points on the unit circle \mathbb{S}^1 . The methods are illustrated with specific data from the jovian moon Europa.

Section 5 contains further technical details and proofs.

2 Directional and axial Gaussian distributions

For a given dimension $d \geq 2$, we consider the space \mathbb{R}^d equipped with standard Euclidean norm $\|\cdot\|$. A directional distribution describes a random unit vector $\mathbf{Y} \in \mathbb{S}^{d-1}$, where $\mathbb{S}^{d-1} = \{\mathbf{y} \in \mathbb{R}^d : \|\mathbf{y}\| = 1\}$. An axial distribution describes a random unit vector $\mathbf{V} \in \mathbb{S}^{d-1}$ with symmetric distribution, where \mathbf{V} represents the random line $\mathbb{R}\mathbf{V}$. In what follows, let M denote the uniform distribution on \mathbb{S}^{d-1} .

2.1 Von Mises–Fisher distributions

The von Mises–Fisher distribution with parameter $\mathbf{z} \in \mathbb{R}^d$, denoted by $\text{vMF}(\mathbf{z})$, is given by the density

$$f_{\mathbf{z}}(\mathbf{y}) := e^{\mathbf{z}^\top \mathbf{y} - \gamma(\mathbf{z})}$$

with respect to M , where $\gamma : \mathbb{R}^d \rightarrow \mathbb{R}$ is the cumulant-generating function of M ,

$$\gamma(\mathbf{z}) := \log \int e^{\mathbf{z}^\top \mathbf{y}} M(d\mathbf{y}).$$

Some authors rather talk about the vMF distribution with concentration parameter $\|\mathbf{z}\|$ and center $\|\mathbf{z}\|^{-1}\mathbf{z}$, see Mardia and Jupp (2000). But in view of the regression methods introduced later, we stick to the parametrization in terms of vectors in \mathbb{R}^d .

The family $(\text{vMF}(\mathbf{z}))_{\mathbf{z} \in \mathbb{R}^d}$ is a natural exponential family, and it is well-known that for a random vector $\mathbf{Y} \sim \text{vMF}(\mathbf{z})$, its mean vector and covariance matrix are given by the gradient and Hessian matrix of γ ,

$$\begin{aligned} \boldsymbol{\mu}(\mathbf{z}) &:= \mathbb{E}(\mathbf{Y}) = \nabla \gamma(\mathbf{z}), \\ \boldsymbol{\Sigma}(\mathbf{z}) &:= \text{Cov}(\mathbf{Y}) = D^2 \gamma(\mathbf{z}). \end{aligned}$$

Other well-known facts are that the mapping $\boldsymbol{\mu} : \mathbb{R}^d \rightarrow \{\mathbf{x} \in \mathbb{R}^d : \|\mathbf{x}\| < 1\}$ is a diffeomorphism, and by means of a Lagrange argument one can show that the density $f_{\mathbf{z}}$ maximizes differential Shannon entropy

$$-\int f(\mathbf{y}) \log f(\mathbf{y}) M(d\mathbf{y})$$

among all probability densities f with respect to M satisfying

$$\int f(\mathbf{y}) \mathbf{y} M(d\mathbf{y}) = \boldsymbol{\mu}(\mathbf{z}).$$

For that reason, some authors refer to the vMF distributions as Gaussian directional distributions, alluding to the fact that any Gaussian density maximizes entropy among all densities with the same first and second moments.

2.2 Bingham distributions

A random axis $\mathbb{R}\mathbf{V}$ in \mathbb{R}^d , given by a random unit vector $\mathbf{V} \in \mathbb{S}^{d-1}$ with symmetric distribution, can be identified with the symmetric matrix $\mathbf{V}\mathbf{V}^\top \in \mathbb{R}^{d \times d}$ describing the orthogonal projection of \mathbb{R}^d onto $\mathbb{R}\mathbf{V}$. Maximizing differential Shannon entropy over all densities f with respect to M such that $\int f(\mathbf{v})\mathbf{v}\mathbf{v}^\top M(d\mathbf{v})$ is a given symmetric matrix with trace 1 leads to the following type of distribution: For a symmetric matrix $\mathbf{W} \in \mathbb{R}^{d \times d}$ with trace 0, the Bingham distribution $\text{Bh}(\mathbf{W})$ has density

$$f_{\mathbf{W}}^{\text{B}}(\mathbf{v}) = e^{\langle \mathbf{v}\mathbf{v}^\top, \mathbf{W} \rangle - \gamma^{\text{B}}(\mathbf{W})} = e^{\mathbf{v}^\top \mathbf{W} \mathbf{v} - \gamma^{\text{B}}(\mathbf{W})},$$

where

$$\gamma^{\text{B}}(\mathbf{W}) := \log \int e^{\mathbf{v}^\top \mathbf{W} \mathbf{v}} M(d\mathbf{v}).$$

Bingham (1974) introduced these distributions for dimension $d = 3$, but the extension to arbitrary dimensions $d \geq 2$ is straightforward. Again, since the density of $\text{Bh}(\mathbf{W})$ maximizes differential Shannon entropy among all probability densities f such that $\int f(\mathbf{v})\mathbf{v}\mathbf{v}^\top M(d\mathbf{v})$ is a given symmetric matrix with trace 1, some authors refer to the Bh distributions as Gaussian axial distributions.

2.3 The special case of $d = 2$

In the special case of the unit circle \mathbb{S}^1 , there is a useful connection between vMF and Bh distributions. Starting from an axis $\mathbb{R}\mathbf{v}$ with $\mathbf{v} \in \mathbb{S}^1$, we rescale and center the corresponding projection matrix $\mathbf{v}\mathbf{v}^\top$ similarly as Arnold and Jupp (2013) and write

$$2\mathbf{v}\mathbf{v}^\top - \mathbf{I}_2 = \begin{bmatrix} 2v_1^2 - 1 & 2v_1v_2 \\ 2v_1v_2 & 2v_2^2 - 1 \end{bmatrix} = \begin{bmatrix} v_1^2 - v_2^2 & 2v_1v_2 \\ 2v_1v_2 & v_2^2 - v_1^2 \end{bmatrix} = \begin{bmatrix} y_1(\mathbf{v}) & y_2(\mathbf{v}) \\ y_2(\mathbf{v}) & -y_1(\mathbf{v}) \end{bmatrix},$$

where

$$\mathbf{y}(\mathbf{v}) := [v_1^2 - v_2^2, 2v_1v_2]^\top \in \mathbb{S}^1. \quad (1)$$

If we identify any vector in \mathbb{R}^2 with a complex number, then $\mathbf{y}(\mathbf{v}) = \mathbf{v}^2$. In particular, this shows immediately that $\|\mathbf{y}(\mathbf{v})\| = 1$. Hence there is a one-to-one correspondence between axes in \mathbb{R}^2 and the unit circle \mathbb{S}^1 , and specifying the expectation $\int \mathbf{v}\mathbf{v}^\top Q(d\mathbf{v})$ for a distribution Q on \mathbb{S}^1 is equivalent to specifying the expectation $\int \mathbf{y}(\mathbf{v}) Q(d\mathbf{v})$. Note further that any symmetric matrix $\mathbf{W} \in \mathbb{R}^{2 \times 2}$ may be written as

$$\mathbf{W} = \begin{bmatrix} z_1 & z_2 \\ z_2 & -z_1 \end{bmatrix}$$

for some $\mathbf{z} \in \mathbb{R}^d$, and elementary algebra reveals that

$$\mathbf{v}^\top \mathbf{W} \mathbf{v} = \mathbf{z}^\top \mathbf{y}(\mathbf{v}).$$

Furthermore, if $\mathbf{V} \sim M$, then $\mathbf{y}(\mathbf{V}) \sim M$ too, and these findings imply the very useful fact that

$$\mathbf{V} \sim \text{Bh}(\mathbf{W}) \quad \text{if and only if} \quad \mathbf{y}(\mathbf{V}) \sim \text{vMF}(\mathbf{z}). \quad (2)$$

To visualize a Bingham distribution $\text{Bh}(\mathbf{W})$, let us resort to random angles. One may write

$$\mathbf{W} = \kappa \begin{bmatrix} \cos(2\beta) & \sin(2\beta) \\ \sin(2\beta) & -\cos(2\beta) \end{bmatrix}$$

for some $\kappa \geq 0$ and some angle $\beta \in [0, \pi)$. If $\mathbf{v} = [\cos(\theta), \sin(\theta)]^\top$ for some angle $\theta \in [0, 2\pi)$, then $\mathbf{y}(\mathbf{v}) = [\cos(2\theta), \sin(2\theta)]^\top$ and

$$\mathbf{v}^\top \mathbf{W} \mathbf{v} = \mathbf{y}(\mathbf{v})^\top \mathbf{z} = \kappa \cos(2(\theta - \beta)).$$

Hence, $\mathbf{V} \sim \text{Bh}(\mathbf{W})$ means that $\mathbf{V} = [\cos(\tilde{V}), \sin(\tilde{V})]^\top$ with a random angle $\tilde{V} \in [0, 2\pi)$ having density

$$\tilde{f}_{\mathbf{w}}(\theta) := e^{\kappa \cos(2(\theta - \beta)) - \tilde{\gamma}(\kappa)} \quad (3)$$

with respect to the uniform distribution on $[0, 2\pi)$, where

$$\tilde{\gamma}(\kappa) := \log \int e^{\kappa y_1} M(d\mathbf{y}) = \log \left(\frac{1}{2\pi} \int_0^{2\pi} e^{\kappa \cos(2(\theta - \beta))} d\theta \right).$$

This shows that in case of $\kappa > 0$, the preferred axis direction is $\pm[\cos(\beta), \sin(\beta)]^\top$, and κ measures the strength of this preference. Thus we reparametrize the Bingham distribution $\text{Bh}(\mathbf{W})$ with the parameter vector

$$\mathbf{w} := \kappa [\cos(\beta), \sin(\beta)]^\top$$

and write $\text{Bh}(\mathbf{w})$ instead of $\text{Bh}(\mathbf{W})$.

Figure 3 depicts the distribution $\text{Bh}(\mathbf{w})$ for two different vectors $\mathbf{w} = \kappa [\cos(\beta), \sin(\beta)]^\top$. One possible representation is the corresponding angular density \tilde{f} in (3). Another possibility is to draw an ‘‘axial histogram’’, that is, the region surrounded by the curve $\theta \mapsto \tilde{f}(\theta)^{1/2} [\cos(\theta), \sin(\theta)]^\top$, leading to a symmetric but non-circular ‘‘pie’’ (unless $\kappa = 0$). The area of any ‘‘slice’’ of this pie with boundary angles $0 \leq \theta_1 < \theta_2 \leq 2\pi$ equals 2π times the probability that $\tilde{V} \in [\theta_1, \theta_2)$.

2.4 Computational aspects of vMF distributions

The function γ . If \mathbf{Y}_0 is a random vector with uniform distribution $M = \text{vMF}(\mathbf{0})$ on \mathbb{S}^{d-1} , then for any unit vector $\mathbf{v} \in \mathbb{S}^{d-1}$, the random variable $U_0 := \mathbf{Y}_0^\top \mathbf{v} \in (-1, 1)$ has density h_d ,

$$h_d(u) := C_d (1 - u^2)^{a_d - 1}, \quad u \in (-1, 1), \quad (4)$$

where $a_d := (d - 1)/2$ and $C_d := 1/B(1/2, a_d)$ with the beta function $B(\cdot, \cdot)$. This implies that

$$\gamma(\mathbf{z}) = \tilde{\gamma}_d(\|\mathbf{z}\|),$$

where

$$\tilde{\gamma}_d(t) := \log G_d(t), \quad G_d(t) := \int_{-1}^1 e^{tu} h_d(u) du$$

for $t \in \mathbb{R}$. The function G_d can also be written as $G_d(t) = t^{1-d/2} J_{d/2-1}(t)$, where J_β stands for the modified Bessel function of the first kind, see Mardia and Jupp (2000). In the special case $d = 3$, $h_3 \equiv 1/2$ and $G_3(t) = \sinh(t)/t$.

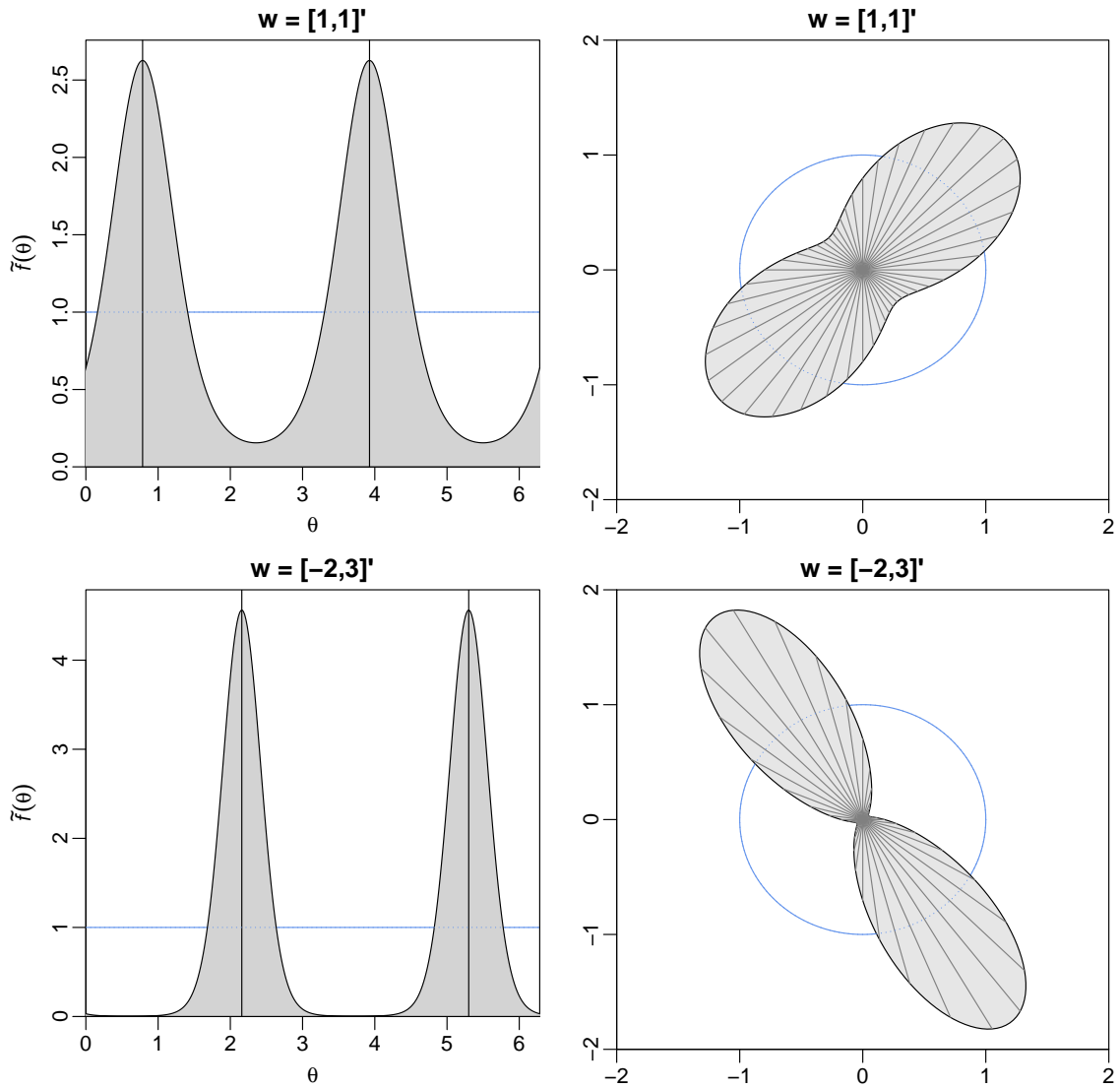


Figure 3: Bingham distributions $\text{Bh}(\mathbf{w})$ for $\mathbf{w} = [1, 1]^\top$ (top row, $\kappa \approx 1.414$, $\beta \approx 0.785$) and $\mathbf{w} = [-2, 3]^\top$ (bottom row, $\kappa \approx 3.606$, $\beta \approx 2.159$). The left column shows the angular densities \tilde{f} , the right column the “axial histograms”.

With our regression applications in mind, we decided to calculate G_d directly, rather than using the detour via Bessel functions. A Taylor series for G_d is given by

$$G_d(t) = \sum_{k=0}^{\infty} c_{d,k} t^{2k} \quad \text{with} \quad c_{d,k} := \frac{2^{-2k} \Gamma(d/2)}{k! \Gamma(k + d/2)}. \quad (5)$$

Mean and Covariance of $\text{vMF}(\mathbf{z})$. Note first that symmetry considerations reveal that $\mathbf{Y}_0 \sim \text{vMF}(\mathbf{0})$ satisfies

$$\mathbb{E}(\mathbf{Y}_0) = \mathbf{0} \quad \text{and} \quad \mathbb{E}(\mathbf{Y}_0 \mathbf{Y}_0^\top) = d^{-1} \mathbf{I}_d.$$

An arbitrary $\mathbf{z} \in \mathbb{R}^d$ may be written as $\mathbf{z} = t\mathbf{v}$ with $t = \|\mathbf{z}\|$ and some $\mathbf{v} \in \mathbb{S}^{d-1}$. Then, $\mathbf{Y}_z \sim \text{vMF}(\mathbf{z})$ may be represented as

$$\mathbf{Y}_z = U_t \mathbf{v} + \sqrt{1 - U_t^2} \mathbf{S}_v,$$

where $U_t \in (-1, 1)$ and $\mathbf{S}_v \in \mathbb{S}^{d-1}$ are stochastically independent, U_t has density $e^{tu - \tilde{\gamma}_d(t)} h_d(u)$ at $u \in (-1, 1)$, and \mathbf{S}_v is uniformly distributed on the unit sphere $\mathbb{S}^{d-1} \cap \mathbf{v}^\perp$ of the $(d-1)$ -dimensional space \mathbf{v}^\perp . In particular, one can deduce from the properties of \mathbf{Y}_0 that $\mathbb{E}(\mathbf{S}_v) = \mathbf{0}$ and $\mathbb{E}(\mathbf{S}_v \mathbf{S}_v^\top) = (d-1)^{-1}(\mathbf{I}_d - \mathbf{v}\mathbf{v}^\top)$. Together with independence of U_t and \mathbf{S}_v we obtain the following formulae for $\boldsymbol{\mu}(\mathbf{z})$ and $\boldsymbol{\Sigma}(\mathbf{z})$:

$$\begin{aligned} \boldsymbol{\mu}(\mathbf{z}) &= \mathbb{E}(U_t) \mathbf{v}, \\ \boldsymbol{\Sigma}(\mathbf{z}) &= \text{Var}(U_t) \mathbf{v}\mathbf{v}^\top + \frac{1 - \mathbb{E}(U_t^2)}{d-1} (\mathbf{I}_d - \mathbf{v}\mathbf{v}^\top). \end{aligned}$$

Note that

$$\mathbb{E}(U_t^\ell) = \int_{-1}^1 u^\ell e^{tu} h_d(u) du / \int_{-1}^1 e^{tu} h_d(u) du = G_d^{(\ell)}(t) / G_d(t)$$

with $G_d^{(\ell)}$ denoting the ℓ -th derivative of G_d . Thus,

$$\begin{aligned} \boldsymbol{\mu}(\mathbf{z}) &= \frac{G_d'(t)}{G_d(t)} \mathbf{v}, \\ \boldsymbol{\Sigma}(\mathbf{z}) &= \left(\frac{G_d''(t)}{G_d(t)} - \left(\frac{G_d'(t)}{G_d(t)} \right)^2 \right) \mathbf{v}\mathbf{v}^\top + \frac{1}{d-1} \left(1 - \frac{G_d''(t)}{G_d(t)} \right) (\mathbf{I}_d - \mathbf{v}\mathbf{v}^\top). \end{aligned}$$

From the series expansion of $G_d(t)$ and the representations $\mathbb{E}(U_t) = \tilde{\gamma}'_d(t)$, $\text{Var}(U_t) = \tilde{\gamma}''_d(t)$ one can deduce expansions of $\gamma(\mathbf{z})$, $\boldsymbol{\mu}(\mathbf{z})$ and $\boldsymbol{\Sigma}(\mathbf{z})$ for \mathbf{z} close to $\mathbf{0}$.

Lemma 1. As $\mathbf{z} \rightarrow \mathbf{0}$,

$$\begin{aligned} \gamma(\mathbf{z}) &= \frac{\|\mathbf{z}\|^2}{2d} - \frac{\|\mathbf{z}\|^4}{4d(d+2)} + O(\|\mathbf{z}\|^6), \\ \boldsymbol{\mu}(\mathbf{z}) &= \frac{1}{d} \left(1 - \frac{\|\mathbf{z}\|^2}{d(d+2)} \right) \mathbf{z} + O(\|\mathbf{z}\|^5), \\ \boldsymbol{\Sigma}(\mathbf{z}) &= \frac{1}{d} \left(1 - \frac{\|\mathbf{z}\|^2}{d(d+2)} \right) \mathbf{I}_d - \frac{2}{d^2(d+2)} \mathbf{z}\mathbf{z}^\top + O(\|\mathbf{z}\|^4). \end{aligned}$$

Numerical computation of $G_d^{(\ell)}(t)$ for moderate values of t . Note first that

$$\frac{c_{d,k+1}t^{2(k+1)}}{c_{d,k}t^{2k}} = \frac{(t/2)^2}{(k+1)(k+d/2)} \quad \text{for } k \geq 0.$$

Consequently,

$$\sum_{k=k_o+1}^{\infty} c_{d,k}t^{2k} \leq \epsilon \quad \text{as soon as} \quad c_{d,k_o}t^{2k_o} \leq \epsilon, \quad \frac{(t/2)^2}{(k_o+1)(k_o+d/2)} \leq 1/2.$$

This allows the computation of $G_d(t)$ with arbitrary prescribed precision.

Any derivative $G_d^{(\ell)}$ can be expressed in terms of G_{d+2m} , $m = 1, \dots, \ell$. Indeed,

$$G_d'(t) = \frac{t}{d} G_{d+2}(t). \quad (6)$$

From this formula, one can proceed inductively. In particular,

$$G_d''(t) = \frac{1}{d} G_{d+2}(t) + \frac{t^2}{d(d+2)} G_{d+4}(t).$$

Computation of $G_d(t)$, $\mathbb{E}(U_t)$ and $\mathbb{E}(U_t^2)$ for large values of t . For large values of t , computing $G_d(t)$, $G_{d+2}(t)$ and $G_{d+4}(t)$ via their series expansion becomes problematic. Here we resort to approximation formulae. The following result is proved in Section 5.

Lemma 2. *Let $z = tv$ with $t > 0$ and $v \in \mathbb{S}^{d-1}$. Then as $t \rightarrow \infty$ and uniformly in v ,*

$$\begin{aligned} \gamma(z) &= \log\left(\frac{2^{a_d-1}\Gamma(d/2)}{\Gamma(1/2)}\right) + t - a_d \log(t) - \frac{a_d(a_d-1)}{2t} \left(1 + \frac{1}{2t} + O(t^{-2})\right), \\ \boldsymbol{\mu}(z) &= \left(1 - \frac{a_d}{t} \left(1 - \frac{a_d-1}{2t} + O(t^{-2})\right)\right) \mathbf{v}, \\ \boldsymbol{\Sigma}(z) &= \frac{a_d}{t^2} \left(1 - \frac{a_d-1}{t} + O(t^{-2})\right) \mathbf{v}\mathbf{v}^\top + \frac{1}{t} \left(1 - \frac{a_d}{t} + O(t^{-2})\right) (\mathbf{I}_d - \mathbf{v}\mathbf{v}^\top). \end{aligned}$$

The formulae in this lemma, without the terms $O(t^{-2})$, provide excellent approximations as soon as $t = \|\mathbf{z}\|$ is larger than, say, $100d$.

3 Regression methods for directional data

Consider observation pairs $(\mathbf{X}_i, \mathbf{Y}_i)$, $1 \leq i \leq n$, consisting of a covariate (vector) \mathbf{X}_i in an arbitrary set \mathcal{X} and a response vector $\mathbf{Y}_i \in \mathbb{S}^{d-1}$ such that

$$\mathcal{L}(\mathbf{Y}_i | \mathbf{X}_1, \dots, \mathbf{X}_n) = \text{vMF}(\mathbf{f}^*(\mathbf{X}_i))$$

for some unknown regression function $\mathbf{f}^* : \mathcal{X} \rightarrow \mathbb{R}^d$. The task is to estimate \mathbf{f}^* from the given data.

3.1 Generalized linear models

A possible parametric approach is to assume that the unknown regression function f^* belongs to a given finite-dimensional space \mathcal{F} of functions $f : \mathcal{X} \rightarrow \mathbb{R}^d$. Conditioning on the covariates \mathbf{X}_i , $1 \leq i \leq n$, and assuming that the responses \mathbf{Y}_i are conditionally independent, the resulting negative log-likelihood function $\ell = \ell(\cdot | \text{data}) : \mathcal{F} \rightarrow \mathbb{R}$ is given by

$$\ell(\mathbf{f}) = \sum_{i=1}^n (\gamma(\mathbf{f}(\mathbf{X}_i)) - \mathbf{Y}_i^\top \mathbf{f}(\mathbf{X}_i)).$$

Specifically, suppose that each function $\mathbf{f} \in \mathcal{F}$ is equal to $\mathbf{f} = (f_k)_{k=1}^d$ with all components f_k belonging to the same finite-dimensional linear space \mathcal{F}^o of functions $f^o : \mathcal{X} \rightarrow \mathbb{R}$. If f_1^o, \dots, f_r^o is a basis of \mathcal{F}^o , then any function $\mathbf{f} \in \mathcal{F}$ can be represented as

$$\mathbf{f}(\mathbf{x}) = \Theta \mathbf{F}^o(\mathbf{x})$$

with a parameter matrix $\Theta \in \mathbb{R}^{d \times r}$ and $\mathbf{F}^o(\mathbf{x}) := (f_j^o(\mathbf{x}))_{j=1}^r \in \mathbb{R}^r$. This leads to the negative log-likelihood function $L : \mathbb{R}^{d \times r} \rightarrow \mathbb{R}$,

$$L(\Theta) := \ell(\Theta \mathbf{F}^o) = \sum_{i=1}^n (\gamma(\Theta \mathbf{F}^o(\mathbf{X}_i)) - \mathbf{Y}_i^\top \Theta \mathbf{F}^o(\mathbf{X}_i)).$$

Since $\boldsymbol{\mu}(z)$ and $\Sigma(z)$ are the gradient and Hessian matrix of γ at z , for $\Theta, \Delta \in \mathbb{R}^{d \times r}$,

$$\begin{aligned} L(\Theta + \Delta) &= L(\Theta) + \sum_{i=1}^n (\boldsymbol{\mu}(\Theta \mathbf{F}^o(\mathbf{X}_i)) - \mathbf{Y}_i)^\top \Delta \mathbf{X}_i \\ &\quad + \frac{1}{2} \sum_{i=1}^n \mathbf{F}^o(\mathbf{X}_i)^\top \Delta^\top \Sigma(\Theta \mathbf{X}_i) \Delta \mathbf{F}^o(\mathbf{X}_i) + O(\|\Delta\|_F^3) \end{aligned}$$

as $\Delta \rightarrow 0$. Here $\|\mathbf{A}\|_F$ is the Frobenius norm of a matrix \mathbf{A} . If we define $\langle \mathbf{A}, \mathbf{B} \rangle = \text{trace}(\mathbf{A}^\top \mathbf{B})$ for matrices \mathbf{A}, \mathbf{B} of the same size, then $\|\mathbf{A}\|_F = \langle \mathbf{A}, \mathbf{A} \rangle^{1/2}$, and

$$\sum_{i=1}^n (\boldsymbol{\mu}(\Theta \mathbf{F}^o(\mathbf{X}_i)) - \mathbf{Y}_i)^\top \Delta \mathbf{F}^o(\mathbf{X}_i) = \langle \Delta, \mathbf{G}(\Theta) \rangle$$

with the gradient matrix

$$\mathbf{G}(\Theta) := \sum_{i=1}^n (\boldsymbol{\mu}(\Theta \mathbf{F}^o(\mathbf{X}_i)) - \mathbf{Y}_i) \mathbf{X}_i^\top \in \mathbb{R}^{d \times r}. \quad (7)$$

Moreover, if $\Delta = [\Delta_1, \dots, \Delta_r]$ with $\Delta_j \in \mathbb{R}^d$, then for $\mathbf{x} \in \mathcal{X}$ and $\Sigma \in \mathbb{R}_{\text{sym}}^{d \times d}$,

$$\mathbf{F}^o(\mathbf{x})^\top \Delta^\top \Sigma \Delta \mathbf{F}^o(\mathbf{x}) = \text{vec}(\Delta)^\top (\mathbf{F}^o(\mathbf{x}) \mathbf{F}^o(\mathbf{x})^\top \otimes \Sigma) \text{vec}(\Delta),$$

where

$$\begin{aligned} \text{vec}(\Delta) &:= [\Delta_1^\top, \Delta_2^\top, \dots, \Delta_r^\top]^\top \in \mathbb{R}^{dr}, \\ \mathbf{F}^o(\mathbf{x}) \mathbf{F}^o(\mathbf{x})^\top \otimes \Sigma &:= \begin{bmatrix} f_1^o(\mathbf{x}) f_1^o(\mathbf{x}) \Sigma & f_1^o(\mathbf{x}) f_2^o(\mathbf{x}) \Sigma & \dots & f_1^o(\mathbf{x}) f_r^o(\mathbf{x}) \Sigma \\ f_2^o(\mathbf{x}) f_1^o(\mathbf{x}) \Sigma & f_2^o(\mathbf{x}) f_2^o(\mathbf{x}) \Sigma & \dots & f_2^o(\mathbf{x}) f_r^o(\mathbf{x}) \Sigma \\ \vdots & \vdots & \ddots & \vdots \\ f_r^o(\mathbf{x}) f_1^o(\mathbf{x}) \Sigma & f_r^o(\mathbf{x}) f_2^o(\mathbf{x}) \Sigma & \dots & f_r^o(\mathbf{x}) f_r^o(\mathbf{x}) \Sigma \end{bmatrix} \in \mathbb{R}_{\text{sym}}^{dr \times dr} \end{aligned}$$

Hence, the Hessian matrix for $L(\Theta)$, viewed as a function of $\text{vec}(\Theta)$, equals

$$\sum_{i=1}^n \mathbf{F}^o(\mathbf{X}_i) \mathbf{F}^o(\mathbf{X}_i)^\top \otimes \Sigma(\Theta \mathbf{X}_i). \quad (8)$$

These formulae are useful to minimize $L(\cdot)$ over $\mathbb{R}^{d \times r}$ via a Newton–Raphson procedure.

3.2 Smoothing via local GLMs

A possible extension of parametric GLMs are nonparametric analyses, where the unknown regression function \mathbf{f}^* is only assumed to be “smooth” and estimated via local parametric models in the spirit of Fan et al. (1998). The value of \mathbf{f}^* at a particular point $\mathbf{x}^o \in \mathcal{X}$ is estimated by $\widehat{\mathbf{f}}(\mathbf{x}^o) = \widehat{\mathbf{f}}_{\mathbf{x}^o}(\mathbf{x}^o)$, where

$$\widehat{\mathbf{f}}_{\mathbf{x}^o}(\cdot) = \arg \min_{\mathbf{f} \in \mathcal{F}} \sum_{i=1}^n w_{\mathbf{x}^o}(\mathbf{X}_i) (\gamma(\mathbf{f}(\mathbf{X}_i)) - \mathbf{Y}_i^\top \mathbf{f}(\mathbf{X}_i))$$

with a certain weight function $w_{\mathbf{x}^o}(\cdot) : \mathcal{X} \rightarrow [0, \infty)$. This leads to a target function $\Theta \mapsto L_{\mathbf{x}^o}(\Theta)$. The only modification in the previous formulae (7) for its gradient and (8) for its Hessian matrix are additional weights $w_{\mathbf{x}^o}(\mathbf{X}_i)$ for all summands in $\sum_{i=1}^n \dots$. Often it is advisable to parametrize the family \mathcal{F} or \mathcal{F}^o locally to improve numerical stability.

Specifically let $\mathcal{X} = \mathbb{R}^q$. For a given number $N \in (0, n)$, one could set

$$w_{\mathbf{x}^o}(\mathbf{x}) = \exp(-S_{\mathbf{x}^o, N} \|\mathbf{x} - \mathbf{x}^o\|^2), \quad (9)$$

where $S_{\mathbf{x}^o, N} > 0$ is chosen such that $\sum_{i=1}^n \exp(-S_{\mathbf{x}^o, N} \|\mathbf{X}_i - \mathbf{x}^o\|^2) = N$.

If \mathcal{F} consists of all constant functions with values in \mathbb{R}^d , then the estimation task is easily solved by

$$\widehat{\mathbf{f}}(\mathbf{x}^o) = \boldsymbol{\mu}^{-1}(\bar{\mathbf{Y}}(\mathbf{x}^o))$$

with the inverse $\boldsymbol{\mu}^{-1} : \{\mathbf{z} \in \mathbb{R}^d : \|\mathbf{z}\| < 1\} \rightarrow \mathbb{R}^d$ of the mean function $\boldsymbol{\mu}(\cdot)$ for vMF distributions.

If \mathcal{F} consists of all linear functions $\mathbf{f} : \mathbb{R}^q \rightarrow \mathbb{R}^d$, then a suitable local basis of \mathcal{F}^o is given by the $r = q + 1$ functions $f_0^o(\mathbf{x}) := 1$ and

$$f_j^o(\mathbf{x}) := x_j - x_{o,j}, \quad 1 \leq j \leq q,$$

with $\mathbf{x}_o = (x_{o,j})_{j=1}^q$.

If \mathcal{F} consists of all quadratic functions $\mathbf{f} : \mathbb{R}^q \rightarrow \mathbb{R}^d$, then these $d + 1$ local basis functions are complemented with the $q(q + 1)/2$ functions

$$f_{jk}^o(\mathbf{x}) := (x_j - x_{o,j})(x_k - x_{o,k}), \quad 1 \leq j \leq k \leq q,$$

so \mathcal{F}^o has dimension $r = (q + 1)(q + 2)/2$.

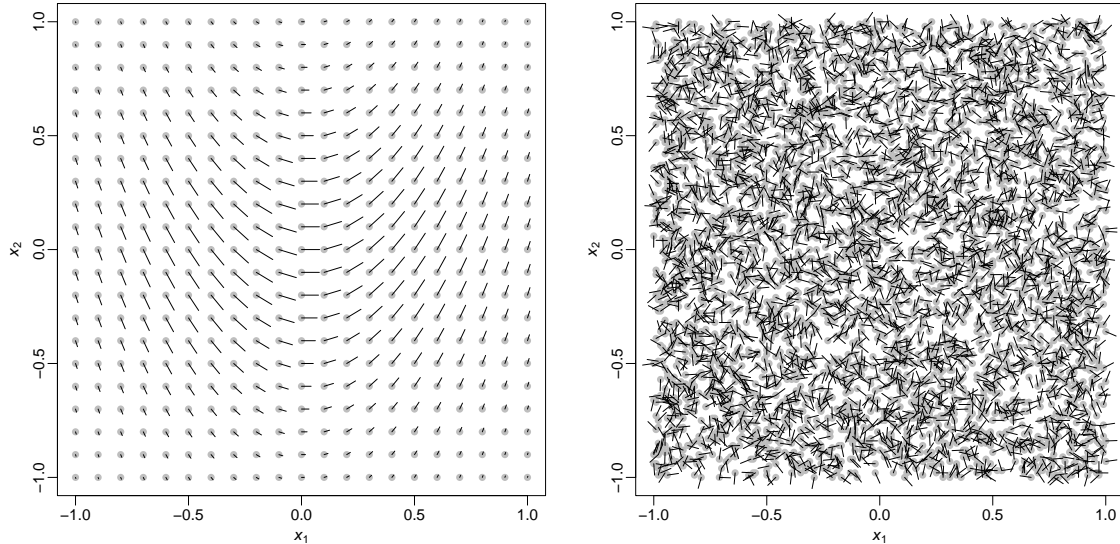


Figure 4: True function \mathbf{f}^* (left panel) and simulated raw data $(\mathbf{X}_i, \mathbf{Y}_i)$ (right panel).

Numerical example. To illustrate these methods, we simulated $n = 4000$ independent observations $(\mathbf{X}_i, \mathbf{Y}_i)$ $1 \leq i \leq n$, such that \mathbf{X}_i is uniformly distributed on $[-1, 1]^2$ while conditional on \mathbf{X}_i , \mathbf{Y}_i follows the vMF distribution with parameter $\mathbf{f}^*(\mathbf{X}_i)$, where

$$\mathbf{f}^*(\mathbf{x}) = \exp(-2\|\mathbf{x}\|^2) \begin{bmatrix} 1 \\ 3x_1 \end{bmatrix}.$$

Figure 4 depicts this function \mathbf{f}^* as a vector field (left panel) and shows the raw data $(\mathbf{X}_i, \mathbf{Y}_i)$ (right panel). For the true function, at each point \mathbf{x}_o on the regular grid $\mathcal{X}_o = \{k/10 : -10 \leq k \leq 10\}^2$ of $21^2 = 441$ points (gray bullets), a line segment connecting \mathbf{x}_o with $\mathbf{x}_o + 0.18 \cdot \boldsymbol{\mu}(\mathbf{f}^*(\mathbf{x}_o))$ is attached (black line). Similarly, at each location \mathbf{X}_i , a line segment connecting \mathbf{X}_i and $\mathbf{X}_i + 0.05 \cdot \mathbf{Y}_i$ is attached.

Figure 5 illustrates the weights $w_{\mathbf{x}_o}(\mathbf{X}_i)$ for two different choices of \mathbf{x}_o and the weights defined via (9) with three different choices for N . The weights $w_{\mathbf{x}_o}(\mathbf{X}_i)$ are coded on a gray scale with 1 corresponding to 1 and almost white corresponding to 0. The coordinates of \mathbf{x}_o are indicated by auxiliary red lines.

The error of a local polynomial estimator $\hat{\mathbf{f}}$ was quantified by

$$\text{RMSE}(\mathbf{f}) := \sqrt{441^{-1} \sum_{\mathbf{x}_o \in \mathcal{X}_o} \|\boldsymbol{\mu}(\hat{\mathbf{f}}(\mathbf{x}_o)) - \boldsymbol{\mu}(\mathbf{f}^*(\mathbf{x}_o))\|^2}.$$

The following table shows $\text{RMSE}(\mathbf{f})$ (rounded to four digits) for the three types of local polynomial estimators and three different values of N :

N	constant	linear	quadratic
100	0.0755	0.0875	0.1279
200	0.0725	0.0704	0.0913
400	0.0902	0.0753	0.0650

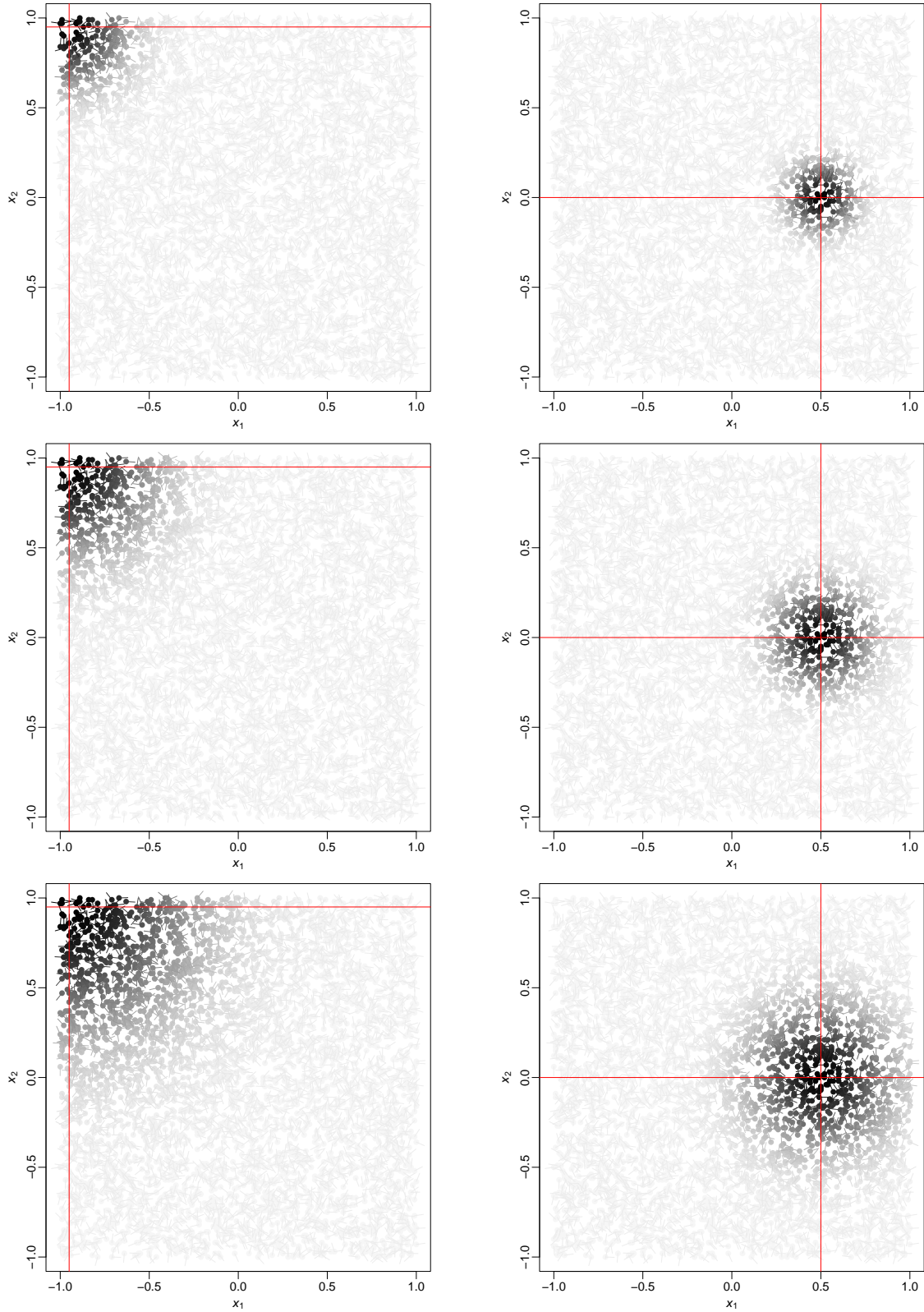


Figure 5: Locally weighted raw data via (9) with $\mathbf{x}_o = [-0.95, 0.95]^\top$ (left column) and $\mathbf{x}_o = [0.5, 0]^\top$ (right column), where $N = 100$ (1st row), $N = 200$ (2nd row) or $N = 400$ (3rd row).

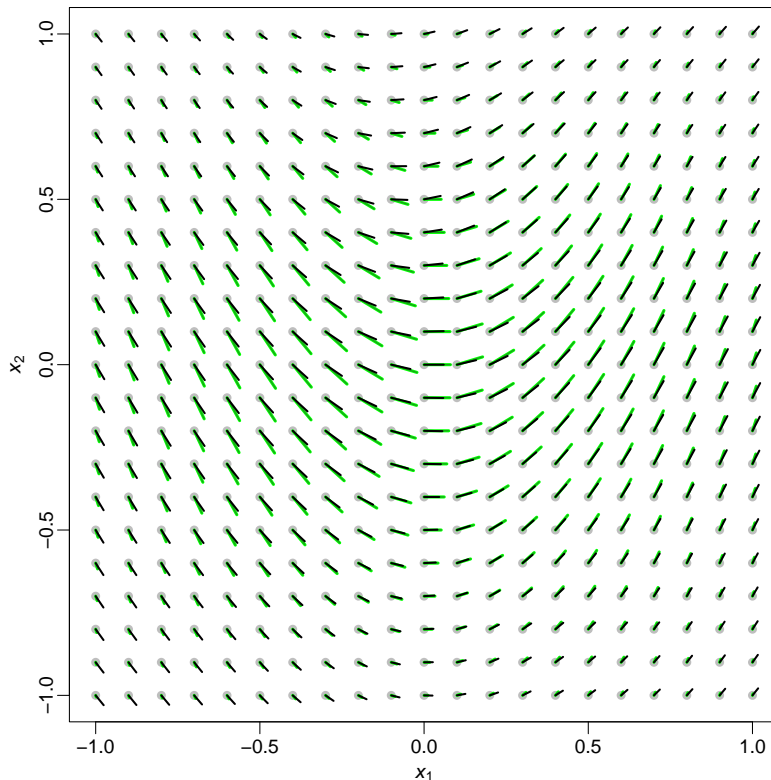


Figure 6: Locally constant fit \hat{f} (black) and f^* (green) in case of $N = 400$.

These numbers reflect only one data set, but they indicate that for $N = 100$, the local constant estimator outperforms the other two. For $N = 200$, the local linear estimator performs best, whereas for $N = 400$, the local quadratic estimator is superior to the other two. Looking at pictures of \hat{f} and f^* , these effects may be explained as in local polynomial least squares regression: For smaller values of N , the local linear and local quadratic estimators tend to overfit the data, whereas for larger values of N , the bias of the local constant or local linear estimator tends to be larger than in case of local quadratic modelling. Figures 6, 7 and 8 depict the three estimators \hat{f} for $N = 400$ (black), together with the true function f^* (green). Looking at these plots carefully, one can see that the local constant estimator seems to be more biased than the other two close to the boundary of $[-1, 1]^2$. On the other hand, the local constant and linear estimators tend to underestimate the norm of $\mu(f^*)$ in the central region, whereas the local quadratic estimator is rather accurate there.

4 Analyzing ice cracks on Europa

We return to a data set consisting of points $(\mathbf{X}_i, \mathbf{V}_i)$, $1 \leq i \leq n$, where $\mathbf{X}_i \in \mathbb{S}^2$ and $\mathbf{V}_i \in \mathbb{S}^2 \cap \mathbf{X}_i^\perp$ representing the axis $\mathbb{R}\mathbf{V}_i$ in the tangent plane of the sphere at \mathbf{X}_i . By means of these observations, we want to fit for any point $\mathbf{x}_o \in \mathbb{S}^3$ a Bingham distribution $\text{Bh}(\mathbf{x}_o, \hat{\mathbf{f}}(\mathbf{x}_o))$, where $\hat{\mathbf{f}}(\mathbf{x}_o) \in \mathbf{x}_o^\perp$. For any vector $\mathbf{w} \in \mathbf{x}_o^\perp$, the Bingham distribution $\text{Bh}(\mathbf{x}_o, \mathbf{w})$ is defined as follows: Let $\mathbf{e}_1, \mathbf{e}_2$ be an orthonormal basis of \mathbf{x}_o^\perp such that the orthogonal matrix $[\mathbf{x}_o, \mathbf{e}_1, \mathbf{e}_2]$ has determinant 1.

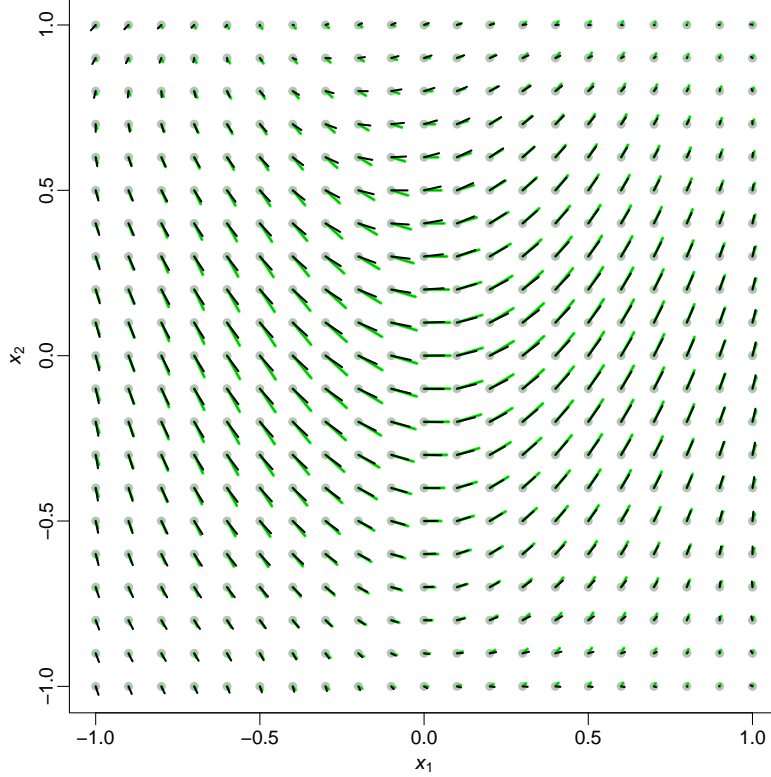


Figure 7: Locally linear fit \hat{f} (black) and f^* (green) in case of $N = 400$.

Writing $\mathbf{w} = \kappa \cos(\beta)\mathbf{e}_1 + \kappa \sin(\beta)\mathbf{e}_2$ for some $\kappa \geq 0$ and $\beta \in [0, \pi)$, the distribution $\text{Bh}(\mathbf{x}_o, \mathbf{w})$ describes the distribution of the random vector

$$\mathbf{V} = \cos(\tilde{V})\mathbf{e}_1 + \sin(\tilde{V})\mathbf{e}_2 \in \mathbf{x}_o^\perp,$$

where $\tilde{V} \in [0, 2\pi)$ is a random variable following the density (3). To relate the observations $(\mathbf{X}_i, \mathbf{V}_i)$ to the point $\mathbf{x}_o \in \mathbb{S}^2$ and its tangent plane \mathbf{x}_o^\perp , we need a suitable transformation which is described in the next two paragraphs.

A stereographic projection. We start with the particular reference point $\mathbf{x}_o = [1, 0, 0]^\top$. Any point $\mathbf{x} \in \mathbb{R}^3$ with $x_1 > -1$ is mapped to a point $P(\mathbf{x}) \in \mathbb{R}^2$ as follows: One moves \mathbf{x} along the straight line connecting the reference point's antipode $[-1, 0, 0]^\top$ and \mathbf{x} such that it hits the hyperplane $\{\mathbf{z} \in \mathbb{R}^3 : z_1 = 1\}$. That is, we need $\nu(\mathbf{x}) \in \mathbb{R}$ such that $(1 - \nu(\mathbf{x}))[-1, 0, 0]^\top + \nu(\mathbf{x})\mathbf{x} = [1, P(\mathbf{x})^\top]^\top$. This leads to

$$P(\mathbf{x}) := \nu(\mathbf{x}) \begin{bmatrix} x_2 \\ x_3 \end{bmatrix} \quad \text{with} \quad \nu(\mathbf{x}) := \frac{2}{1 + x_1}.$$

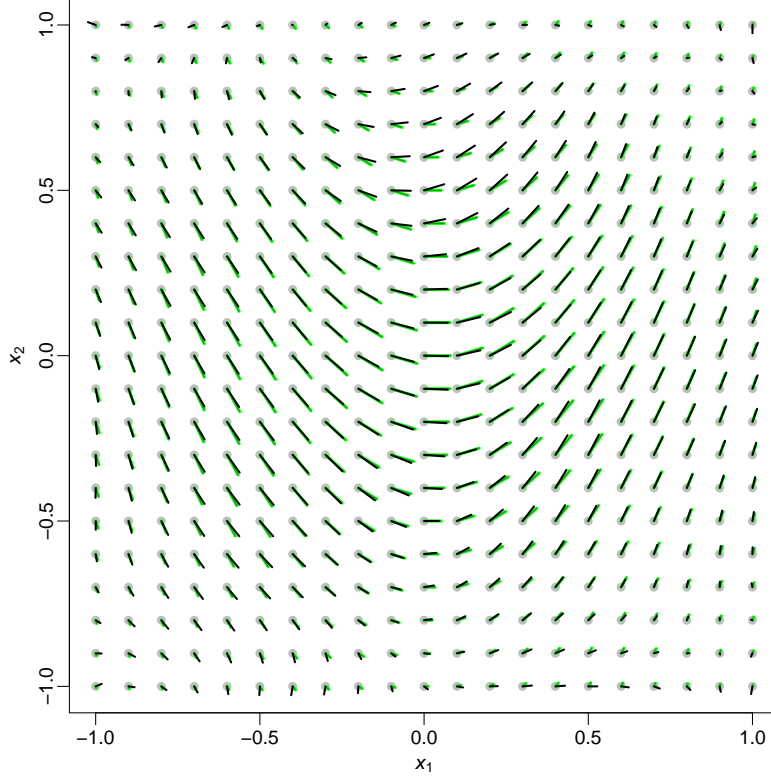


Figure 8: Locally quadratic fit \hat{f} (black) and f^* (green) in case of $N = 400$.

If restricted to $\mathcal{X} := \mathbb{S}^2 \setminus \{[-1, 0, 0]^\top\}$, the mapping $P : \mathcal{X} \rightarrow \mathbb{R}^2$ is a diffeomorphism, and its inverse mapping $P^{-1} : \mathbb{R}^2 \rightarrow \mathcal{X}$ is given by

$$P^{-1}(\mathbf{z}) := \begin{bmatrix} 2\omega(\mathbf{z}) - 1 \\ \omega(\mathbf{z})z_1 \\ \omega(\mathbf{z})z_2 \end{bmatrix} \quad \text{with} \quad \omega(\mathbf{z}) := \frac{4}{4 + \|\mathbf{z}\|^2}.$$

For $\mathbf{x} \in \mathcal{X}$, any vector $\mathbf{v} \in \mathbf{x}^\perp$ can be viewed as the derivative of a smooth curve in \mathbb{S}^2 passing through \mathbf{x} , so it is natural to consider $DP(\mathbf{x})\mathbf{v}$ with the Jacobian matrix $DP(\mathbf{x}) \in \mathbb{R}^{2 \times 3}$. Elementary calculations show that

$$DP(\mathbf{x}) = \nu(\mathbf{x})\mathbf{A}(\mathbf{x}) \quad \text{with} \quad \mathbf{A}(\mathbf{x}) := \begin{bmatrix} -x_2/(1+x_1) & 1 & 0 \\ -x_3/(1+x_1) & 0 & 1 \end{bmatrix}.$$

It is well-known that P is a conformal mapping in the sense that $DP(\mathbf{x}) : \mathbf{x}^\perp \rightarrow \mathbb{R}^2$ preserves angles. Precisely, one can show that for arbitrary $\mathbf{v} \in \mathbf{x}^\perp$,

$$\|\mathbf{A}(\mathbf{x})\mathbf{v}\|^2 = \|\mathbf{v}\|^2.$$

Thus we relate the pair (\mathbf{x}, \mathbf{v}) to the reference point $[1, 0, 0]^\top$ and its tangent plane by mapping it to the pair

$$(P(\mathbf{x}), \mathbf{A}(\mathbf{x})\mathbf{v}) \in \mathbb{R}^2 \times \mathbb{R}^2.$$

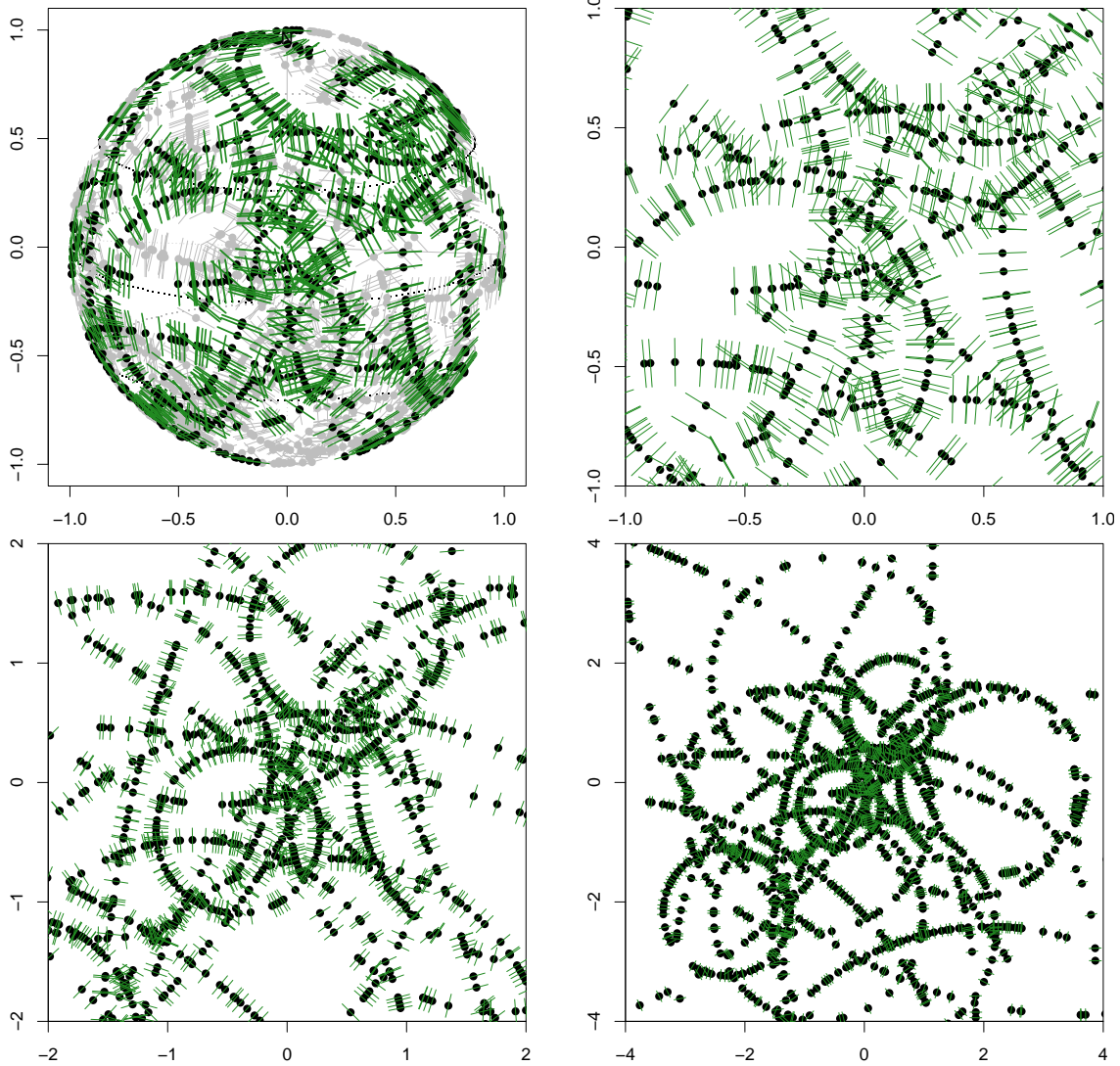


Figure 9: Stereographic projections of an artificial data set. Top left: full sphere. Others: stereographic projection at different scales, showing that it is conformal.

Figure 9 illustrates this mapping. The upper left panel shows an artificial set of points $(\mathbf{X}_i, \mathbf{V}_i)$, $1 \leq i \leq n$, where $\mathbf{X}_i \in \mathbb{S}^2$ and $\mathbf{V}_i \in \mathbb{S}^2 \cap \mathbf{X}_i^\perp$. The axes correspond to the second and third components of all vectors. Note that the data points \mathbf{X}_i (black dots) are situated on a finite collection of circles on \mathbb{S}^2 , and each axis \mathbf{V}_i (indicated by a green line connecting $\mathbf{X}_i \pm 0.1 \cdot \mathbf{V}_i$) is perpendicular to the circle containing \mathbf{X}_i . The other panels show the projected points $(P(\mathbf{X}_i), A(\mathbf{X}_i)\mathbf{V}_i)$ in squares of different size centered around $\mathbf{0}$. One sees clearly the conformal nature of this projection and the well-known fact that circles are mapped onto circles.

Smoothing the data for an arbitrary reference point. For an arbitrary reference point $\mathbf{x}_o \in \mathbb{S}^2$, we choose an orthogonal matrix B_o with determinant 1 such that $B_o \mathbf{x}_o = [1, 0, 0]^\top$. Then all data

points $(\mathbf{X}_i, \mathbf{V}_i)$ with $\mathbf{X}_i \neq -\mathbf{x}_o$ are transformed into the pairs

$$(P(\mathbf{B}_o \mathbf{X}_i), \mathbf{A}(\mathbf{B}_o \mathbf{X}_i) \mathbf{B}_o \mathbf{V}_i) \in \mathbb{R}^2 \times \mathbb{S}^1.$$

Since $\mathbf{A}(\mathbf{B}_o \mathbf{X}_i) \mathbf{B}_o \mathbf{V}_i$ represents an axis in \mathbb{R}^2 , we replace it by means of the mapping $\mathbf{y}(\cdot)$ in (1) with the direction $\mathbf{y}(\mathbf{A}(\mathbf{B}_o \mathbf{X}_i) \mathbf{B}_o \mathbf{V}_i) \in \mathbb{S}^1$. Then we apply the local polynomial estimators described in Section 3.2 to the data pairs $(P(\mathbf{B}_o \mathbf{X}_i), \mathbf{y}(\mathbf{A}(\mathbf{B}_o \mathbf{X}_i) \mathbf{B}_o \mathbf{V}_i)) \in \mathbb{R}^2 \times \mathbb{S}^1$ and $\mathbf{0}$ in place of $(\mathbf{X}_i, \mathbf{Y}_i)$ and \mathbf{x}_o . This yields an estimated vMF parameter $\hat{\mathbf{z}} \in \mathbb{R}^2$. Writing $\hat{\mathbf{z}} = \hat{\kappa}[\cos(2\hat{\beta}), \sin(2\hat{\beta})]^\top$ with $\hat{\kappa} \geq 0$ and $\hat{\beta} \in [0, \pi)$, we replace $\hat{\mathbf{z}}$ with the axis parameter $\hat{\mathbf{w}} := \hat{\kappa}[\cos(\hat{\beta}), \sin(\hat{\beta})]^\top$ and transform it back to the Bingham parameter

$$\hat{\mathbf{f}}(\mathbf{x}_o) := \mathbf{B}_o^\top \begin{bmatrix} 0 \\ \hat{\mathbf{w}} \end{bmatrix} \in \mathbf{x}_o^\perp.$$

This leads to the estimate $\text{Bh}(\mathbf{x}_o, \hat{\mathbf{f}}(\mathbf{x}_o))$ of $\text{Bh}(\mathbf{x}_o, \mathbf{f}^*(\mathbf{x}_o))$. Note that any choice of \mathbf{B}_o would yield the same estimate $\text{Bh}(\mathbf{x}_o, \hat{\mathbf{f}}(\mathbf{x}_o))$.

Some numerical results for Europa. We analyzed the data from Europa and determined Bingham distributions $\text{Bh}(\mathbf{x}_o, \hat{\mathbf{f}}(\mathbf{x}_o))$ for many different locations \mathbf{x}_o . Precisely, within each of the 19 regions, we chose an evenly spread subset of size up to 200 of all observed locations \mathbf{X}_i there. For the parameter N we used 100, 200 and 400. Now we show some results for the particular region in Figure 2. Since the results for the three values of N look very similar, we only show the ones for $N = 200$ in Figure 10. The upper left panel shows only the 200 selected points \mathbf{x}_o . These coincide with the selected 200 points \mathbf{X}_i in Figure 2, but for the computation of $\hat{\mathbf{f}}$ we used all 2656 data pairs from that region. The other three panels depict the fitted Bingham distributions by means of local constant, linear and quadratic modelling. Each distribution $\text{Bh}(\mathbf{x}_o, \hat{\mathbf{f}}(\mathbf{x}_o))$ is represented by a blue line segment connecting the points

$$\mathbf{x}_o \pm 0.1 \cdot \boldsymbol{\mu}(\hat{\mathbf{f}}(\mathbf{x}_o)) = \mathbf{x}_o \pm 0.1 \cdot \tilde{\gamma}'_2(\hat{\kappa}(\mathbf{x}_o)) \hat{\mathbf{u}}(\mathbf{x}_o),$$

where $\hat{\kappa}(\mathbf{x}_o)$ and $\hat{\mathbf{u}}(\mathbf{x}_o)$ are the norm and direction of $\hat{\mathbf{f}}(\mathbf{x}_o)$, respectively. Recall that for each estimate $\hat{\mathbf{f}}(\mathbf{x}_o)$, a new stereographic projection with reference point \mathbf{x}_o was used.

In the upper part of the chosen region, the direction of the ice cracks seems to be rather chaotic (i.e. uniform), whereas in the middle and lower parts, there are preferred axis directions. These findings supplement observations by the physicists (Haslebacher et al., 2025) who analysed the region divided into geological chaos terrain (upper part) and ridged plains (middle and lower part) by Leonard et al. (2024). It is an interesting finding that in the chaos terrain, no “order” is found in the sense of a preferred crack direction. To which extent tidal forces enforce cracking is still under debate.

Some final comments. The starting point for the present manuscript was the data from Europa. But as mentioned before, analogous questions arise with observations from Ganymede (Rossi et al., 2020). In the latter case, the axes refer to grooves (i.e. tectonic deformations) rather than

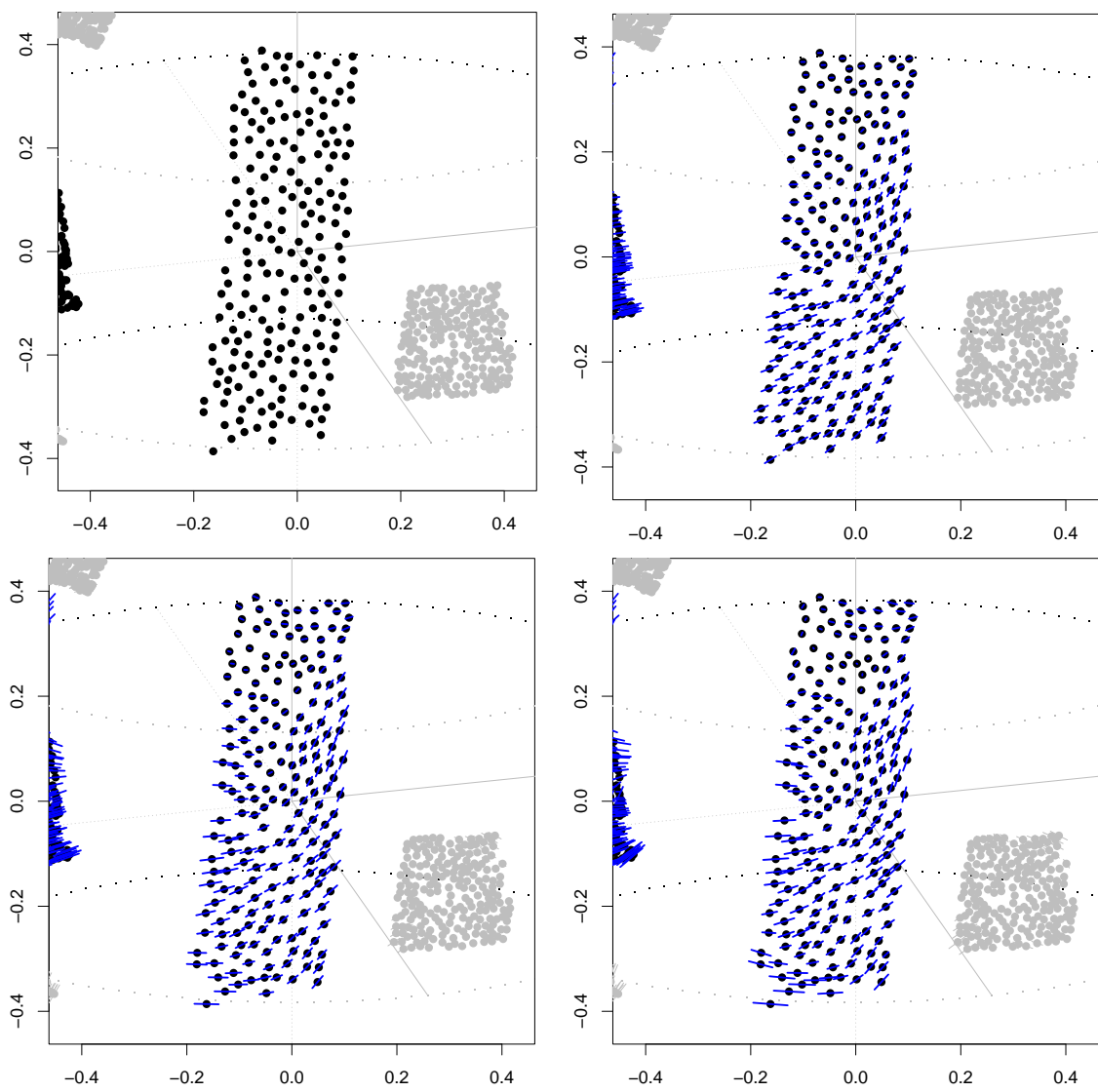


Figure 10: Smoothed data from Europa with $N = 200$: Locations only (top left) and fitted parameter vectors via local constant (top right), linear (bottom left) and quadratic (bottom right) modelling.

cracks. We are currently experimenting with data from Ganymede and planning to compare our results with previous ones. There are also potential applications for planets with non-icy surfaces, e.g. faults in the solid surface of Mercury (Watters et al., 2001) or Venus (Sabbeth et al., 2023).

In the derivation of the regression and smoothing methods, we used the standard setting of stochastically independent responses, given the covariates. For the application to Europa or Ganymede, this assumption is certainly not satisfied, for instance, because very long ice cracks lead to several observations $(\mathbf{X}_i, \mathbf{V}_i)$ with different locations \mathbf{X}_i but similar axis directions \mathbf{V}_i . Thus, the methods presented here are merely exploratory and serve to find and visualize patterns in the data, without statistical conclusions such as standard errors, p-values or confidence bounds.

The simulations and data analyses were carried out with the programming language R (R Core Team, 2023). The code we used is available from the first author upon request.

5 Technical details

Proof of (4). Let $\mathbf{Z} \in \mathbb{R}^d$ be a standard Gaussian random vector. Then, $\mathbf{Y}_0^\top \mathbf{v}$ has the same distribution as $Z_1/\|\mathbf{Z}\|$, and $Z_1^2/\|\mathbf{Z}\|^2$ follows $\text{Beta}(1/2, a_d)$. Denoting the density of the latter distribution with b_d , it follows from the symmetry of the distribution of $Z_1/\|\mathbf{Z}\|$ that for $u \in (0, 1)$,

$$h_d(u) = -\frac{d}{du} \mathbb{P}(Z_1/\|\mathbf{Z}\| > u) = -\frac{d}{du} 2^{-1} \mathbb{P}(Z_1^2/\|\mathbf{Z}\|^2 > u^2) = ub_d(u^2),$$

whereas for $u \in (-1, 0)$,

$$h_d(u) = \frac{d}{du} \mathbb{P}(Z_1/\|\mathbf{Z}\| < u) = \frac{d}{du} 2^{-1} \mathbb{P}(Z_1^2/\|\mathbf{Z}\|^2 > u^2) = |u|b_d(u^2).$$

In both cases the result equals $C_d(1 - u^2)^{a_d-1}$, because $b_d(x) = C_dx^{-1/2}(1 - x)^{a_d-1}$ for $x \in (0, 1)$. \square

Proof of (5). Since h_d is even, we may rewrite $G_d(t) = \int_{-1}^1 e^{tu} h_d(u) du$ as

$$\begin{aligned} G_d(t) &= C_d \int_{-1}^1 \cosh(tu)(1 - u^2)^{a_d-1} du \\ &= 2C_d \int_0^1 \cosh(tu)(1 - u^2)^{a_d-1} du \\ &= 2C_d \sum_{k=0}^{\infty} \frac{t^{2k}}{(2k)!} \int_0^1 u^{2k}(1 - u^2)^{a_d-1} du \\ &= C_d \sum_{k=0}^{\infty} \frac{t^{2k}}{(2k)!} \int_0^1 s^{k-1/2}(1 - s)^{a_d-1} ds \quad (s = u^2, 2 du = s^{-1/2} ds) \\ &= \sum_{k=0}^{\infty} c_{d,k} t^{2k}, \end{aligned}$$

where

$$\begin{aligned}
c_{d,k} &:= \frac{1}{(2k)!} \frac{B(k+1/2, a_d)}{B(1/2, a_d)} \\
&= \frac{1}{(2k)!} \frac{\Gamma(k+1/2)}{\Gamma(1/2)} \frac{\Gamma(d/2)}{\Gamma(k+d/2)} \\
&= \frac{2^{-(2k-1)} \Gamma(2k)}{(2k)! \Gamma(k)} \frac{\Gamma(d/2)}{\Gamma(k+d/2)} \\
&= \frac{2^{-(2k-1)} (2k-1)!}{(2k)! (k-1)!} \frac{\Gamma(d/2)}{\Gamma(k+d/2)} \\
&= \frac{2^{-2k} \Gamma(d/2)}{k! \Gamma(k+d/2)},
\end{aligned}$$

where the second step is a consequence of Legendre's well-known duplication formula for the gamma function. \square

Proof of Lemma 1. Note that $G_d(t) = 1 + t^2/(2d) + t^4/(8d(d+2)) + O(t^6)$, whence

$$\begin{aligned}
\tilde{\gamma}_d(t) &= \log\left(1 + \frac{t^2}{2d} + \frac{t^4}{8d(d+2)} + O(t^6)\right) \\
&= \frac{t^2}{2d} + \frac{t^4}{8d(d+2)} - \frac{t^2}{8d^2} + O(t^6) \\
&= \frac{t^2}{2d} - \frac{t^4}{4d^2(d+2)} + O(t^6),
\end{aligned}$$

because $\log(1+x) = x - x^2/2 + O(x^3)$ as $x \rightarrow 0$. Since $\gamma(\mathbf{z}) = \tilde{\gamma}_d(\|\mathbf{z}\|)$, this implies the asserted expansion for $\gamma(\mathbf{z})$. Moreover, since $\tilde{\gamma}_d$ is an analytic function,

$$\begin{aligned}
\mathbb{E}(U_t) &= \tilde{\gamma}'_d(t) = \frac{t}{d} - \frac{t^3}{d^2(d+2)} + O(t^5) = \frac{t}{d} \left(1 - \frac{t^2}{d(d+2)}\right) + O(t^5), \\
\text{Var}(U_t) &= \tilde{\gamma}''_d(t) = \frac{1}{d} - \frac{3t^2}{d^2(d+2)} + O(t^4) = \frac{1}{d} \left(1 - \frac{3t^2}{d(d+2)}\right) + O(t^4).
\end{aligned}$$

Writing $\mathbf{z} = t\mathbf{v}$ with $t = \|\mathbf{z}\|$ and $\mathbf{v} \in \mathbb{S}^{d-1}$, this shows that

$$\boldsymbol{\mu}(\mathbf{z}) = \mathbb{E}(U_t)\mathbf{v} = \frac{1}{d} \left(1 - \frac{\|\mathbf{z}\|^2}{d(d+2)}\right) \mathbf{z} + O(\|\mathbf{z}\|^5).$$

Furthermore,

$$\begin{aligned}
\frac{1 - \mathbb{E}(U_t^2)}{d-1} &= \frac{1 - \text{Var}(U_t) - \mathbb{E}(U_t)^2}{d-1} \\
&= \frac{1}{d-1} \left(1 - \frac{1}{d} + \frac{3t^2}{d^2(d+2)} - \frac{t^2}{d^2}\right) + O(t^4) \\
&= \frac{1}{d-1} \left(\frac{d-1}{d} - \frac{(d-1)t^2}{d^2(d+2)}\right) + O(t^4) \\
&= \frac{1}{d} \left(1 - \frac{t^2}{d(d+2)}\right) + O(t^4),
\end{aligned}$$

whence

$$\begin{aligned}
\Sigma(\mathbf{z}) &= \text{Var}(U_t) \mathbf{v}\mathbf{v}^\top + \frac{1 - \mathbb{E}(U_t^2)}{d-1} (\mathbf{I}_d - \mathbf{v}\mathbf{v}^\top) \\
&= \frac{1}{d} \left(1 - \frac{3\|\mathbf{z}\|^2}{d(d+2)}\right) \mathbf{v}\mathbf{v}^\top + \frac{1}{d} \left(1 - \frac{\|\mathbf{z}\|^2}{d(d+2)}\right) (\mathbf{I}_d - \mathbf{v}\mathbf{v}^\top) + O(\|\mathbf{z}\|^4) \\
&= \frac{1}{d} \left(1 - \frac{\|\mathbf{z}\|^2}{d(d+2)}\right) \mathbf{I}_d - \frac{2}{d^2(d+2)} \mathbf{z}\mathbf{z}^\top + O(\|\mathbf{z}\|^4).
\end{aligned}$$

□

Proof of (6). Starting from the Taylor series of G_d ,

$$\begin{aligned}
G'_d(t) &= \sum_{k=1}^{\infty} 2kc_{d,k} t^{2k-1} \\
&= \sum_{k=1}^{\infty} \frac{2k2^{-2k} \Gamma(d/2)}{k! \Gamma(k+d/2)} t^{2k-1} \\
&= \sum_{k=1}^{\infty} \frac{2^{-2k+1} \Gamma(d/2)}{(k-1)! \Gamma(k+d/2)} t^{2k-1} \\
&= \frac{t \Gamma(d/2)}{2\Gamma(d/2+1)} \sum_{k=1}^{\infty} \frac{2^{-2(k-1)} \Gamma((d+2)/2)}{(k-1)! \Gamma((k-1)+(d+2)/2)} t^{2(k-1)} \\
&= \frac{t}{d} G_{d+2}(t).
\end{aligned}$$

□

For the proof of Lemma 2, we use a general result about expansions of moments for distributions on $(-1, 1)$.

Lemma 3. Let $h : (-1, 1) \rightarrow \mathbb{R}$ be integrable such that for some $k \in \mathbb{N}_0$ and constants $a > 0$ and $b_0, \dots, b_k \in \mathbb{R}$,

$$h(1-r) = \sum_{j=0}^k b_j r^{a+j-1} + O(r^{a+k})$$

as $r \downarrow 0$. Then, for $\ell \in \mathbb{N}_0$,

$$\int_{-1}^1 (1-u)^\ell e^{tu} h(u) du = \Gamma(\ell+a) e^t t^{-(\ell+a)} \left(\sum_{j=0}^k b_j [\ell+a+j-1]_j t^{-j} + O(t^{-(k+1)}) \right)$$

as $t \rightarrow \infty$.

Here and throughout this section, we write $[b]_0 := 1$ and $[b]_j := \prod_{i=0}^{j-1} (b-i)$ for real numbers b and integers $j \geq 1$.

Proof of Lemma 3. We may write

$$\int_{-1}^1 (1-u)^\ell e^{tu} h(u) du = e^t \int_{-1}^1 (1-u)^\ell e^{-t(1-u)} h(u) du = e^t \int_0^2 r^\ell e^{-tr} h(1-r) dr.$$

For any fixed $\delta \in (0, 2)$,

$$\int_0^2 r^\ell e^{-tr} h(1-r) dr = \int_0^\delta r^\ell e^{-tr} h(1-r) dr + R_1(\delta, t)$$

with

$$|R_1(\delta, t)| \leq 2^\ell \int_{-1}^1 |h(u)| du e^{-t\delta} = O(e^{-t\delta}).$$

Moreover,

$$\int_0^\delta r^\ell e^{-tr} h(1-r) dr = \sum_{j=0}^k b_j \int_0^\delta r^{\ell+a+j-1} e^{-tr} dr + R_2(\delta, t),$$

where

$$|R_2(\delta, t)| \leq D(\delta) \int_0^\infty r^{\ell+a+k} e^{-tr} dr = D(\delta) \Gamma(\ell+a+k+1) t^{-(\ell+a+k+1)},$$

and

$$D(\delta) := \sup_{r \in (0, \delta)} r^{-(a+k)} \left| h(1-r) - \sum_{j=0}^k b_j r^{a+j-1} \right|$$

is finite for sufficiently small $\delta > 0$.

Finally,

$$\begin{aligned} \int_0^\delta r^{\ell+a+j-1} e^{-tr} dr &= t^{-(\ell+a+j)} \int_0^{t\delta} y^{\ell+a+j-1} e^{-y} dy \\ &= \Gamma(\ell+a+j) t^{-(\ell+a+j)} + O(t^{-(\ell+a+j)} e^{-\delta t/2}), \end{aligned}$$

because for any $m > 0$ and a random variable Y with distribution $\text{Gamma}(m, 1)$, it follows from Markov's inequality that

$$\int_{t\delta}^\infty y^{m-1} e^{-y} dy = \Gamma(m) \mathbb{P}(G_m \geq t\delta) \leq \Gamma(m) \mathbb{E}(e^{G_m/2}) e^{-t\delta/2} = \Gamma(m) 2^m e^{-t\delta/2}.$$

The asserted expansion is now a consequence of the fact that $\Gamma(\ell+a+j) = [\ell+a+j-1]_j \Gamma(\ell+a)$ for integers $j \geq 0$. \square

Lemma 3 will be applied to the particular density h_d , noting that

$$\begin{aligned} h_d(1-r) &= C_d (2r - r^2)^{a_d-1} \\ &= 2^{a_d-1} C_d r^{a_d-1} (1-r/2)^{a_d-1} \\ &= \frac{2^{a_d-1} \Gamma(d/2)}{\Gamma(a_d) \Gamma(1/2)} r^{a_d-1} \left(1 - \frac{a_d-1}{2} r + \frac{[a_d-1]_2}{8} r^2 + O(r^3) \right) \end{aligned} \quad (10)$$

as $r \downarrow 0$. Applying Lemma 3 to h_d with the latter expansion leads to expansions for $G_d(t)$ and $\log G_d(t)$.

Corollary 4. As $t \rightarrow \infty$,

$$G_d(t) = \frac{2^{a_d-1}\Gamma(d/2)}{\Gamma(1/2)} e^{t-t^{a_d}} \left(1 - \frac{[a_d]_2}{2t} + \frac{[a_d+1]_4}{8t^2} + O(t^{-3})\right)$$

and

$$\log G_d(t) = \log\left(\frac{2^{a_d-1}\Gamma(d/2)}{\Gamma(1/2)}\right) + t - a_d \log(t) - \frac{[a_d]_2}{2t} \left(1 + \frac{1}{2t} + O(t^{-2})\right).$$

Proof of Corollary 4. By means of (10) we can apply Lemma 3 with $h = h_d$, $a = a_d$, $k = 2$ and

$$\begin{aligned} (b_0, b_1, b_2) &= 2^{a_d-1} C_d \left(1, -\frac{a_d-1}{2}, \frac{[a_d-1]_2}{8}\right) \\ &= \frac{2^{a_d-1}\Gamma(d/2)}{\Gamma(a_d)\Gamma(1/2)} \left(1, -\frac{a_d-1}{2}, \frac{[a_d-1]_2}{8}\right). \end{aligned}$$

Then, Lemma 3 implies that

$$\begin{aligned} G_d(t) &= \frac{2^{a_d-1}\Gamma(d/2)}{\Gamma(1/2)} e^{t-t^{a_d}} \left(1 - \frac{a_d(a_d-1)}{2t} + \frac{[a_d+1]_2[a_d-1]_2}{8t^2} + O(t^{-3})\right) \\ &= \frac{2^{a_d-1}\Gamma(d/2)}{\Gamma(1/2)} e^{t-t^{a_d}} \left(1 - \frac{[a_d]_2}{2t} + \frac{[a_d+1]_4}{8t^2} + O(t^{-3})\right), \end{aligned}$$

where these and the subsequent expansions are meant as $t \rightarrow \infty$. Moreover,

$$\log G_d(t) = \log\left(\frac{2^{a_d-1}\Gamma(d/2)}{\Gamma(1/2)}\right) + t - a_d \log(t) + \log\left(1 - \frac{[a_d]_2}{2t} + \frac{[a_d+1]_4}{8t^2} + O(t^{-3})\right),$$

and the standard expansion $\log(1+x) = x - x^2/2 + O(x^3)$ as $x \rightarrow 0$ implies that

$$\begin{aligned} \log\left(1 - \frac{[a_d]_2}{2t} + \frac{[a_d+1]_4}{8t^2} + O(t^{-3})\right) &= -\frac{[a_d]_2}{2t} + \frac{[a_d+1]_4}{8t^2} - \frac{[a_d]_2^2}{8t^2} + O(t^{-3}) \\ &= -\frac{[a_d]_2}{2t} - \frac{[a_d]_2}{4t^2} + O(t^{-3}) \\ &= -\frac{[a_d]_2}{2t} \left(1 + \frac{1}{2t} + O(t^{-2})\right), \end{aligned}$$

because $[a_d+1]_4 - [a_d]_2^2 = -2[a_d]_2$. □

Another consequence are expansions for moments of U_t . Precisely, we can express moments of U_t in terms of moments of $1 - U_t$, and the latter may be approximated by means of Lemma 3.

Corollary 5. As $t \rightarrow \infty$,

$$\begin{aligned} \mathbb{E}(U_t) &= 1 - \frac{a_d}{t} \left(1 - \frac{a_d-1}{2t} + O(t^{-2})\right), \\ \text{Var}(U_t) &= \frac{a_d}{t^2} \left(1 - \frac{a_d-1}{t} + O(t^{-2})\right), \\ \frac{1 - \mathbb{E}(U_t^2)}{d-1} &= \frac{1}{t} \left(1 - \frac{a_d}{t} + O(t^{-2})\right). \end{aligned}$$

Proof of Corollary 5. We apply Lemma 3 with $h = h_d$, $a = a_d$, $k = 1$ and $(b_0, b_1) = C(1, \tilde{b}_1)$ for some constant $C > 0$ and $\tilde{b}_1 = -(a_d - 1)/2$. Note that Lemma 3 implies that for any integer $\ell \geq 1$,

$$\begin{aligned}\mathbb{E}[(1 - U_t)^\ell] &= \int_{-1}^1 (1 - u)^\ell e^{tu} h_d(u) du / \int_{-1}^1 e^{tu} h_d(u) du \\ &= \frac{\Gamma(a_d + \ell)}{\Gamma(a_d)} \frac{1 + \tilde{b}_1(\ell + a_d)t^{-1} + O(t^{-2})}{1 + \tilde{b}_1 a_d t^{-1} + O(t^{-2})} \\ &= \frac{[a_d + \ell - 1]_\ell}{t^\ell} \left(1 + \frac{\tilde{b}_1 \ell}{t} + O(t^{-2})\right) \\ &= \frac{[a_d + \ell - 1]_\ell}{t^\ell} \left(1 - \frac{\ell(a_d - 1)}{2t} + O(t^{-2})\right),\end{aligned}$$

Specifically, for $\ell = 1, 2$ we obtain the expansions

$$\begin{aligned}\mathbb{E}(1 - U_t) &= \frac{a_d}{t} \left(1 - \frac{a_d - 1}{2t} + O(t^{-2})\right), \\ \mathbb{E}[(1 - U_t)^2] &= \frac{[a_d + 1]_2}{t^2} \left(1 - \frac{a_d - 1}{t} + O(t^{-2})\right),\end{aligned}$$

and this implies that

$$\begin{aligned}\text{Var}(U_t) &= \mathbb{E}[(1 - U_t)^2] - [\mathbb{E}(1 - U_t)]^2 \\ &= \frac{[a_d + 1]_2}{t^2} \left(1 - \frac{a_d - 1}{t} + O(t^{-2})\right) - \frac{a_d^2}{t^2} \left(1 - \frac{a_d - 1}{2t} + O(t^{-2})\right)^2 \\ &= \frac{[a_d + 1]_2}{t^2} \left(1 - \frac{a_d - 1}{t} + O(t^{-2})\right) - \frac{a_d^2}{t^2} \left(1 - \frac{a_d - 1}{t} + O(t^{-2})\right) \\ &= \frac{a_d}{t^2} \left(1 - \frac{a_d - 1}{t} + O(t^{-2})\right), \\ 1 - \mathbb{E}(U_t^2) &= 2 \mathbb{E}(1 - U_t) - \mathbb{E}[(1 - U_t)^2] \\ &= \frac{2a_d}{t} - \frac{[a_d]_2}{t^2} - \frac{[a_d + 1]_2}{t^2} + O(t^{-3}) \\ &= \frac{2a_d}{t} - \frac{2a_d^2}{t^2} + O(t^{-3}) \\ &= \frac{d - 1}{t} \left(1 - \frac{a_d}{t} + O(t^{-2})\right),\end{aligned}$$

because $2a_d = d - 1$. □

Lemma 1 is now a direct consequence of Corollaries 4 and 5.

Acknowledgements. The authors are grateful to Riccardo Gatto and Rudy Beran for stimulating discussions and useful references about directional data. Many thanks also to Alyssa Rhoden and Costanza Rossi for sharing data and insights about Europa and Ganymede, respectively, and their interest in the methods presented here.

C. Haslebacher acknowledges financial support of the Swiss National Science Foundation (SNSF) through grants P500PT_225447 and 51NF40_205606. L. Dümbgen acknowledges the support of SNSF through grant 10001553.

References

- ARNOLD, R. and JUPP, P. E. (2013). Statistics of orthogonal axial frames. *Biometrika* **100** 571–586.
- BINGHAM, C. (1974). An antipodally symmetric distribution on the sphere. *Ann. Statist.* **2** 1201–1225.
- FAN, J., FARMEN, M. and GIJBELS, I. (1998). Local maximum likelihood estimation and inference. *J. R. Stat. Soc. Ser. B Stat. Methodol.* **60** 591–608.
- HASLEBACHER, C., TEJERO, J. G., PROCKTER, L. M., LEONARD, E. J., RHODEN, A. R. and THOMAS, N. (2025). Length, width, and relative age analysis of lineaments in the Galileo regional maps with lineamapper. *PSJ* under review.
- HASLEBACHER, C., THOMAS, N. and BICKEL, V. T. (2024). Lineamapper: A deep learning-powered tool for mapping linear surface features on europa. *Icarus* **410**.
- LEONARD, E. J., PATTHOFF, A. D. and SENSKE, D. A. (2024). Global geologic map of europa. *USGS/NASA* 3513.
- MARDIA, K. V. and JUPP, P. E. (2000). *Directional statistics*. Wiley Series in Probability and Statistics, John Wiley & Sons, Ltd., Chichester.
- MCCULLAGH, P. and NELDER, J. A. (1989). *Generalized linear models*. 2nd ed. Monographs on Statistics and Applied Probability, Chapman & Hall, London.
- PEWSEY, A. and GARCÍA-PORTUGUÉS, E. (2021). Recent advances in directional statistics. *TEST* **30** 1–58.
- R CORE TEAM (2023). *R: A Language and Environment for Statistical Computing*. R Foundation for Statistical Computing, Vienna, Austria.
URL <https://www.R-project.org/>
- RHODEN, A. R. and HURFORD, T. A. (2013). Lineament azimuths on europa: Implications for obliquity and non-synchronous rotation. *Icarus* **226** 841–859.
- ROSSI, C., CIANFARRA, P. and SALVINI, F. (2020). Structural geology of ganymede regional groove systems (60°n-60°s). *Journal of Maps* **16** 6–16.
- SABBETH, L., SMREKAR, S. E. and STOCK, J. M. (2023). Estimated seismicity of venusian wrinkle ridges based on fault scaling relationships. *Earth and Planetary Science Letters* **619** 118308.
- WATTERS, T. R., COOK, A. C. and ROBINSON, M. S. (2001). Large-scale lobate scarps in the southern hemisphere of mercury. *Planetary and Space Science* **49** 1523–1530.